Journal of Zhejiang University-SCIENCE A (Applied Physics & Engineering)
ISSN 1673-565X (Print); ISSN 1862-1775 (Online)
www.zju.edu.cn/jzus; www.springerlink.com
E-mail: jzus@zju.edu.cn

Numerical investigation of the convex effect on the behavior of crossing excavations*

Min ZHANG†, Xing-hua WANG†‡, Guang-cheng YANG, You WANG

(*School of Civil Engineering, Central South University, Changsha 410075, China*)

†E-mail: zhangmin021410@126.com; xhwang@mail.csu.edu.cn

Received Feb. 7, 2011; Revision accepted June 7, 2011; Crosschecked Sept. 8, 2011

Abstract: A 3D numerical model considering the soil-structure interaction is presented in this paper to examine the ground movement and internal force during the construction of Qingdao North Metro Station, China with a special focus on the convex effect of the crossing excavation. The influence of intersection angles and soil resilience characteristics on deformation behavior is discussed, and the suitability of two alternative constitutive models applied in excavation simulation is also considered. The analysis results show that a notable convex effect appears to be associated with the crossing excavation, and the intersection is the key area requiring special attention. The displacements at the corner decrease with increasing crossing angles. The axial loads of struts along the retaining pile wall are unequal, and the values near the cross section are generally larger than the average loads of the left-sided ones. The modified Cam-Clay (MCC) model, which is capable of describing the loading-unloading criterion and identifying the stiffness difference of strain hardening between loading and unloading, can yield a relatively high accuracy of estimation for the behavior of excavations in comparison to the Mohr-Coulomb (MC) model. Furthermore, slight soil deformation resilience after unloading can reduce the ground surface settlement and enhance the ground stability.

Key words: Crossing excavation, Convex effect, Constitutive model, Numerical simulation
doi:10.1631/jzus.A1100028 **Document code:** A **CLC number:** TU473

1 Introduction

The convex corner in excavation is often encountered during the construction of an interchange metro station or in the situation of a change in excavation width. In relation to the common concave location, which is beneficial for the excavation stability, the convex effect, instead usually yields a complex stress state, and is often a dangerous area with stress concentration. The unloading resulting from two excavated sides at the intersection strongly affects the soil stress state and stress path, and even causes a wedge-shaped tensile failure involving a decreasing safety factor of stability. The deformation and stability of the retaining structures at the site should be given special attention during design and construction (Wu and Tu, 2007).

It can be expected that the deformation behavior of the pile wall would be greatly influenced by the existence of the corner. Plane strain analyses might give conservative results especially for the center section of a relatively short excavation wall (Ou *et al*., 1996). The spatial effects in excavation have been studied by many researches (Ng and Yan, 1999; Zhang *et al*., 1999; Gourvenec and Powrie, 2000; Finno and Roboski, 2005). Ou and Shiau (1998) found that the wall deformation at the short wall was smaller than that at the long wall, and the wall deformation decreased as the distance from the concave corner decreased. Some 3D finite element analyses have been conducted to predict the performance of the excavation of the north square of Shanghai South Railway Station, China, and the effects of the anisotropic soil stiffness, the adjacent excavation, and zone excavation on the wall

‡ Corresponding author

* Project (No. 2007AA11Z134) supported by the National High-Tech R&D Program (863) of China

deformation have been investigated (Hou *et al*., 2009). The discontinuity of the pile wall along the excavated sides, the effects of wall stiffness in different coordinate directions and rotational fixity in the corner of the excavation were examined by Zdravkovic *et al*. (2005). In this paper, both square and rectangular excavations are compared with the equivalent axisymmetric and plane strain analyses to provide a detailed assessment of wall and ground movements. In addition, when the ground improvement is selected as an auxiliary measure to reduce excavation induced movements, the effect of corner restriction should be properly considered to determine the improved zone reasonably to reach a balance between cost and safety (Ou *et al*., 2008). However, most previous studies focused mainly on the existence of the concave corner, and little information is available concerning the mechanics and deformation behavior during crossing excavation.

According to Tang and Kung (2010), the selection of an adequate soil model that is capable of adequately describing the stress-strain-strength characteristics of the soils is essentially crucial when predicting the excavation-induced ground response. The most important feature of the soil is its stiffness dependent on the stress state and a large stiffness for unloading just as the case of excavation in the study. Recently, to guarantee a sufficient predictive accuracy during excavation, probabilistic analysis conducted by the random finite element method (RFEM) (Tang, 2011) or more advanced constitutive models have taken into account the soil properties of unloading in numerical simulation, such as the t_{ij} model (Nakai *et al*., 2007), hardening-soil (HS) model (Kung and Jheng, 2010), and hardening-small-strain (HSS) model (Benz, 2007; Kung and Jheng, 2010). In addition, the discrepancy among the three types of models, i.e., the Perfect Plasticity model, the HS model and the Consistance et Localisation Explicite (CLoE) model, on wall displacement and surface settlement was analyzed by Viggiani and Tamagnini (2000). It was recommended one use strain hardening plastic constitutive models in excavation simulation to reflect the soil features of plasticity, strain hardening, difference between loading and unloading stiffness, and stress-dependent stiffness (Xu and Wang, 2010).

In this paper, a 3D numerical model using FLAC^{3D} (Fast Lagrangian Analysis of Continua) is developed to study the performance of the crossing excavation behavior of the Qingdao North Metro Station, China, with special focus on the convex effect. The influences of intersection angles and soil resilience characteristic on deformation behavior are discussed and the load state in struts at different distances from the intersection is investigated. Furthermore, the suitability of two alternative approaches of the modified Cam-Clay (MCC) model and Mohr-Coulomb (MC) model representing, respectively, the hardening plasticity and elastic-perfectly plasticity, is also considered in predicting excavation-induced ground movement profiles.

2 Convex effects in excavation

To verify the convex effect on the excavation behavior, several relatively simple cases with different intersection angles ranging from 0° to 270° are considered. For all cases, the mucky soil as well as its properties in the subsequent case history, are adopted here and modeled as an isotropic MCC plastic material. Additionally, the excavation with a fixed depth of 2 m is supported with no retaining structures, intentionally to understand the effect more clearly.

The horizontal displacement distribution, in the case of 90° in Fig. 1, indicates that the soil deflections in the vicinity of the intersection are obviously larger than those on the center section, and an apparent wedge-shaped slide similar to the soil slope appears. The results further confirm that the intersection is the weakest zone during the excavation. The variations of the displacement ratios δ_h and δ_v with different corner angles are presented in Fig. 2, where δ_h and δ_v respectively, represent the horizontal and vertical displacements at the corner to those not at the corner or under plane strain condition, namely the case of 180°. The results reveal that the convex effect plays an influential role on the deformation behavior, and both displacement ratios, which decrease with the increase in the intersection angle, are almost identical to each other, especially as exceeding the 90°. The ratios δ_h and δ_v with the angle 90° are equal to about 3.0; that is to say, the displacement at the convex location is three times that with where there is no corner. However, once the angle exceeds 180°, the corner with convex

shape turns into concave and the excavation induced soil deflection near the corner is constrained. For the right angle, as usually seen in the rectangular excavation, i.e., the angle of 270° in this study, both ratios are equal to only 0.17. It can be inferred that the obtuse angle is a better choice for the crossing excavation if available, including enhancement of propping stiffness or ground improvement.

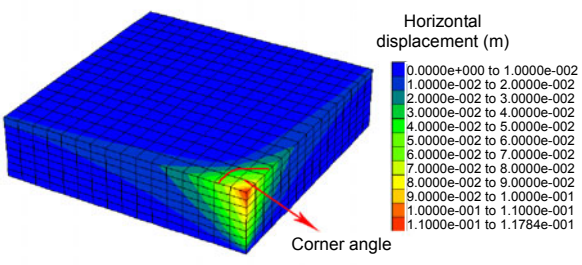

Fig. 1 Horizontal displacement distribution (90°)

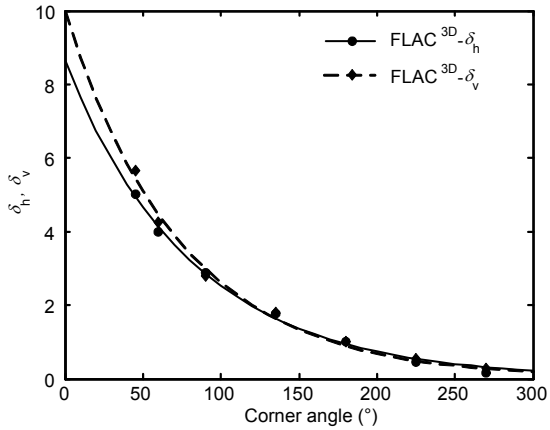

Fig. 2 Relationship between the displacement ratios δ_h, δ_v and the corner angle

3 Case history

The North Metro Station excavation project, which is located on Licang district of Qingdao, is an interchange station of metro Lines No. 1 and No. 3, which cross each other at a right angle. A basement garage of 250 m×160 m and a maximum excavation depth of 10 m, is located on the top of the interchange station. The total layout shows a form of excavation embedded within another, as shown in Fig. 3. The excavation zone formed by coastal marshes of estuarine deposit is now a waste landfill site with open terrain. According to the site investigation report, the subsurface consists of an 8-m thick fill layer Q_4^{ml} of quaternary, which is mainly construction waste, garbage and other miscellaneous fill. Beneath the fill layer, there is a 7.5 m thick silty clay layer Q_4^{m} of marine deposit. The subsequent soil layer is fully weathered mucky sandstone. The ground water level for the excavation site is at ground level (GL) from −0.6 to −5.4 m, and a grouting curtain technology was adopted in front of excavation for water proofing.

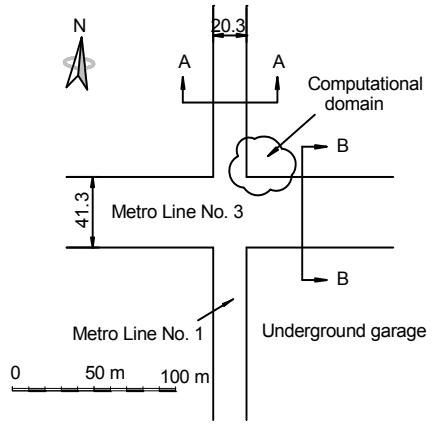

Fig. 3 The location of the excavation site

A bored pile wall, 1.0 m in diameter and 20.7 m and 13.5 m in depth for metro Lines No. 1 and No. 3 respectively, was applied as the earth-retaining system for both excavations in relation to the stratigraphy. A ramp with an aspect ratio of 1:0.6 (height to width) was placed to provide access to the soil transportation during the excavation of metro Line No. 1. To meet the resulting deeper excavation, two groups of three piles with 20 and 16 m depths were installed within a range of 9 m near the intersection. A mechanical deep mixing method was employed to strengthen the inter-pile soil and, in addition, to provide water proofing. Figs. 4 and 5 show the retaining structures of the excavation in cross sections A–A and B–B, respectively. The respective maximum excavation depths of metro Lines No. 1 and No. 3 were 14.7 and 7.0 m from the bottom of the basement garage. As a top-down construction method was adopted, the pile wall in the metro Line No. 1 (Fig. 4) was supported by three levels of steel tube struts spaced at 3 m horizontally with the type of B609×150. As shown in Fig. 5, two levels of tieback anchors consisted a four high strength strand provided lateral support on the other wall in metro Line No. 3. The anchors were

installed at a same spacing as the piles and locked off to a pre-stress of 100 kN.

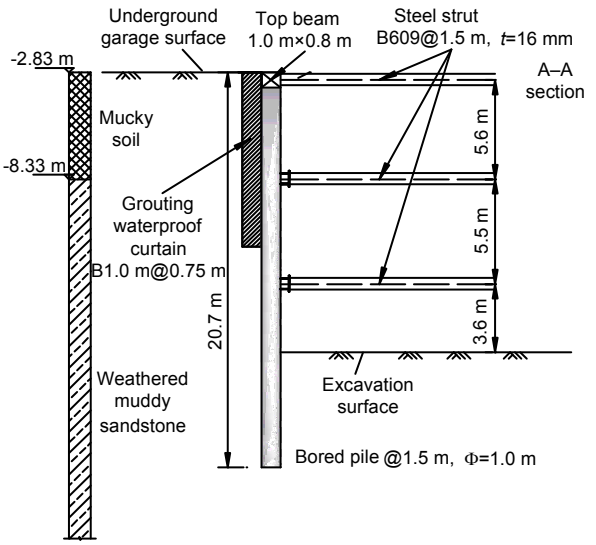

Fig. 4 Cross section A–A of the excavation

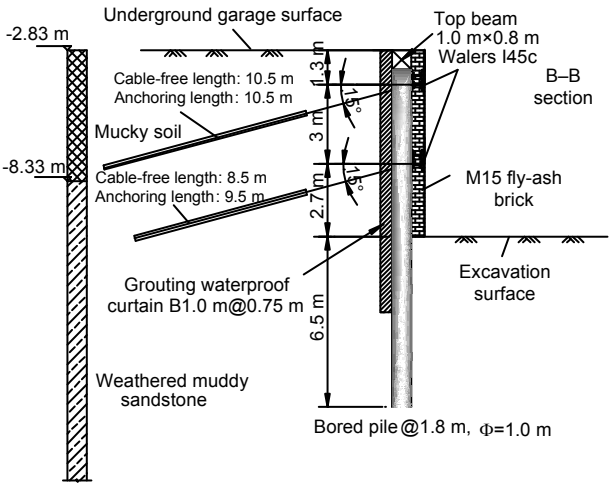

Fig. 5 Cross section B–B of the excavation

The total construction sequences are divided into two stages, the former stage is to excavate the upper parking site and the latter to excavate the interchange station. Seven major construction stages for the later excavation of the interchange station are defined as follows:

1. Stage 1: install pile walls of both metro lines.

2. Stage 2: excavate to GL −2.3 m and install the first level of steel struts in metro Line No. 1 together with the anchors in metro Line No. 3 and then pre-stress.

3. Stage 3: excavate to GL −4.5 m and install the second level of anchors and then pre-stress.

4. Stage 4: excavate to GL −7.0 m, i.e., the bottom of metro Line No. 3, and install the second level of steel struts in metro Line No. 1 together with the anchors near the cross section in metro Line No. 3 and then pre-stress.

5. Stage 5: excavate to GL −9.6 m for the remaining excavation of metro Line No. 1.

6. Stage 6: excavate to GL −12.2 m and install the third level of steel struts in metro Line No. 1.

7. Stage 7: excavate to the bottom (GL −14.7 m) of metro Line No. 1.

Note that the aforementioned GLs are relative to the reference of the bottom of the parking site rather than the original ground surface.

4 Numerical model

As the upper underground parking site was completed in advance and all the excavated sides were far away from the interchange station, its impact on the subsequent excavation of the cross section could be neglected and only the intersection (Fig. 1) was examined in the numerical model. Due to the symmetry with respect to the two central axes of the excavation site, a quarter of the site was used to establish the mesh for the 3D analysis. The meshes of the entire model with overall sizes of $-10\ \text{m}\le x\le 16.2\ \text{m}$, $-9\ \text{m}\le y\le 26\ \text{m}$, $-58\ \text{m}\le z\le 0$ and the retaining structures are shown in Fig. 6. This large zone is selected to avoid any measurable effects from the boundary in the final results. The analyzed zone has 18030 brick elements and 20181 nodes in total. At the bottom level of the computational domain, all movements are restrained while at the lateral external sides, lateral movements perpendicular to the boundary are prohibited. The struts and Walers of the structure are simulated by beam elements, while the pile walls and anchors are modeled using pile and cable elements, respectively.

The mucky soil and weathered sandstone are assumed to be normally consolidated soils behaving as an elastic-plastic body with the modified Cambridge failure criterion described by Roscoe and Burland (1968), and obeying the associated flow rule. The yield surface and the stress-strain behavior are governed by three independent laboratorial parameters, λ, κ, and M, where λ is the slope of normal consolidation line, κ is the slope of elastic swelling line

and M is the frictional constant. The two parameters λ and κ can be derived from an oedometer test, making certain assumptions, M can be obtained through a series of triaxial tests (drained or undrained with pore-pressure measurement), and all of them can be determined by

$$\lambda=\frac{C_c}{\ln 10},\quad \kappa=\frac{C_s}{\ln 10},\quad M=\frac{6\sin\varphi_c'}{3-\sin\varphi_c'}, \tag{1}$$

where C_c is the compression index; C_s is the swelling coefficient, usually chosen in the range of one-fifth to one-third of λ (Itasca Consulting Group, Inc., 2005); and φ_c' is the effective stress critical state friction angle. The relevant material properties of the soil layers at the site are summarized in Table 1. The shear strength and compressive modulus were obtained from consolidated drained (CD) tests and oedometer tests at stress ranging from 100 to 300 kPa, respectively. The parameters C_c and C_s were determined by the semi-logarithmic plot v_e-ln$p$ of a typical isotropic compression test, where v_e is the evolution volume ratio of the soil skeleton to the solid particles, and p is the normal consolidation pressure. These laboratory tests were carried out on thin-walled tube samples retrieved from the retained ground.

The retaining structures are modeled as isotropic linear-elastic materials. The Young's modulus and Poisson's ratio are taken as 30 GPa and 0.2 for the concrete, and 211 GPa and 0.3 for steel, respectively. Note that although the mechanical deep mixing method was employed for water proofing and to strengthen the inter-pile soil in an extent, its retaining contribution is slight in reducing the excavation induced movement. Thus, the soil mixing column behind the pile wall is not considered for simplification, nor is the influence of the ground water.

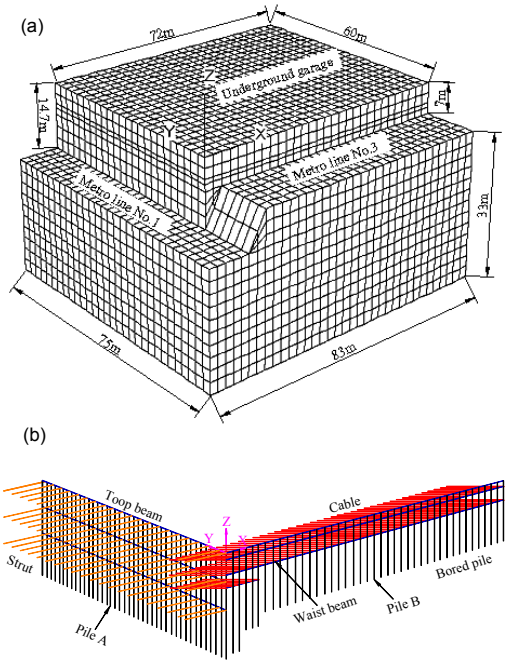

Fig. 6 Mesh of the 3D finite-difference model (a) and the retaining structures (b) of the crossing excavation

5 Experimental

5.1 Deformation analysis

Fig. 7 presents the spatial deformation of the piles along both directions of the metro lines. As an effective propping from the steel struts used in the metro Line No. 1, the displacements of the piles have no significant difference from each other, except at the cross section, where a little larger deformation appears at the tip of the pile (Fig. 7a). And the maximum pile deflection along the metro Line No. 3, contrary to the expectation, does not locate at the crossing site. The typical convex effect as discussed above has also not appeared (Fig. 7b). The reason is that, as compared to the center section, one more level of pre-stressed anchors are added to the piles near the intersection and the deflections are also restrained by the top beam and two levels of Walers from the metro Line No. 1. The results show that the designed propping system together with the method of layered excavation in this case is sufficient to control soil

Table 1 Soil parameters used in numerical analysis

Soil type	ρ (kN/m^3)	E (MPa)	c' (kPa)	φ_c' (°)	$a_{v0.1\text{-}0.2}$	Model parameter				
						λ	κ	e_0	M	ν
Mucky soil	19.0	12	13.2	8.3	0.47	0.031	0.008	0.89	0.303	0.38
Weathered mucky sandstone	19.2	15	28.0	20.1	0.38	0.025	0.006	0.82	0.776	0.35

ρ is the mass density; E is the Young's modulus; c' is the effective stress critical state cohesion; $a_{v0.1\text{-}0.2}$ is the compression coefficient under 0.1–0.2 MPa; e_0 is the initial void ratio; and ν is Poisson's ratio

deformation and diminish the convex effect at the intersection. The spatial form and bending moments (M_y and M_z) of the pile at the corner after excavation are illustrated in Figs. 8a and 8b, respectively. Due to being subject to two horizontal earth stresses, the internal forces of the pile are rather complicated and of the same order of magnitude in both directions. These characteristics of stress and deformation should be fully taken into consideration in design.

Fig. 9 shows the calculated deflections of piles A and B after removing soil at each excavation stage. As shown in Fig. 9a, the pile deflection shows a typical lateral bulging form of a strutted retaining structure and the maximum pile deflections occur near the excavation surface. The pile deflections, being equal to almost zero at the top, are linked to the strong limit by the upper struts. Furthermore, as illustrated in Fig. 9a, the embedment depth of the pile does not appear to have a significant effect on the behavior of the pile and the surrounding soil, as can be found in Zdravkovic *et al*. (2005). These results from the analysis of a deep pile wall can be used to assess the behavior of shallow excavations retained by shallower pile walls. As shown in Fig. 9b, the deflection shape of pile B in metro Line No. 3 behaviors a cantilever form and the maximum wall deflection (approximately 17 mm) on the top of the pile at the final stage, is lower than the value without pre-stress. Due to no existing structures in this case, it is not necessary to assess the risk of damage especially for buildings with less resistance to lateral ground displacements. However, some visible cracks behind the pile wall may generate owing to large surface displacement, which would create a sense of insecurity. Thus, it is still essential to impose the pre-stress on these anchors.

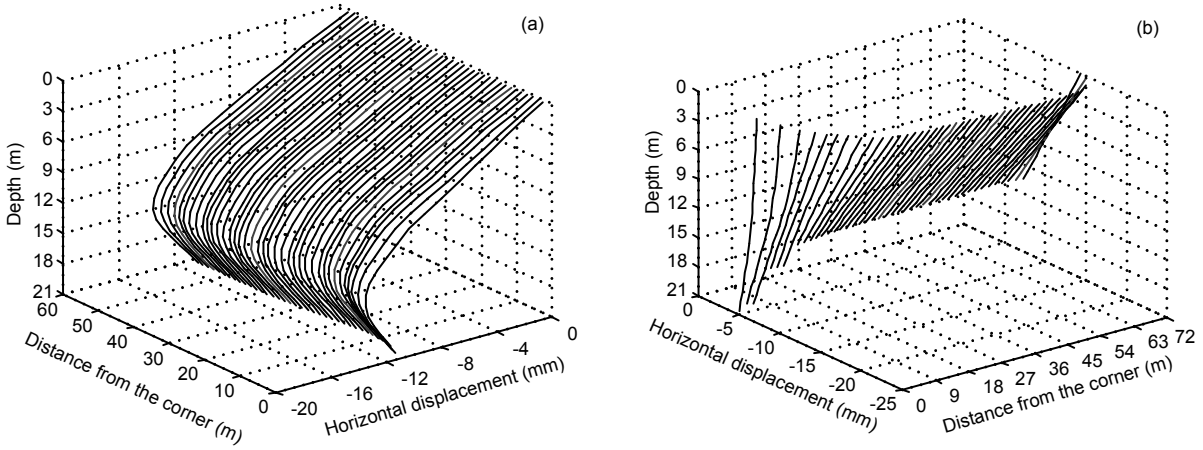

Fig. 7 Spatial forms of the piles along metro Lines No. 1 (a) and No. 3 (b) after excavation

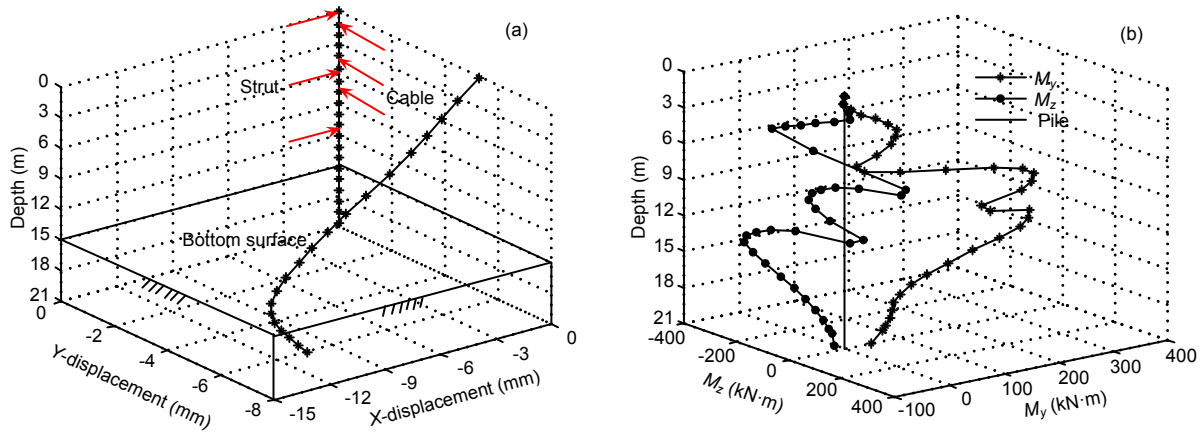

Fig. 8 Spatial deformation (a) and bending moments (b) of the pile at corner

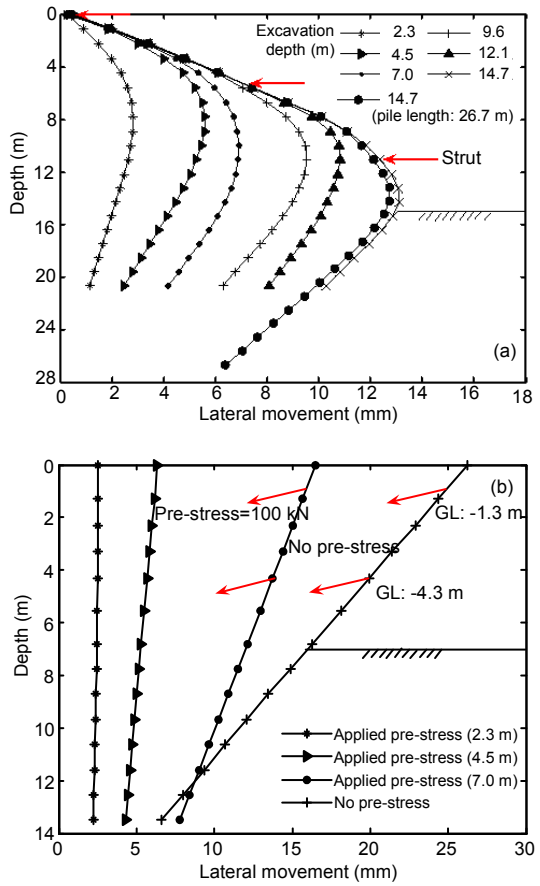

Fig. 9 Deformations of pile A (a) and pile B (b) at different excavation depths

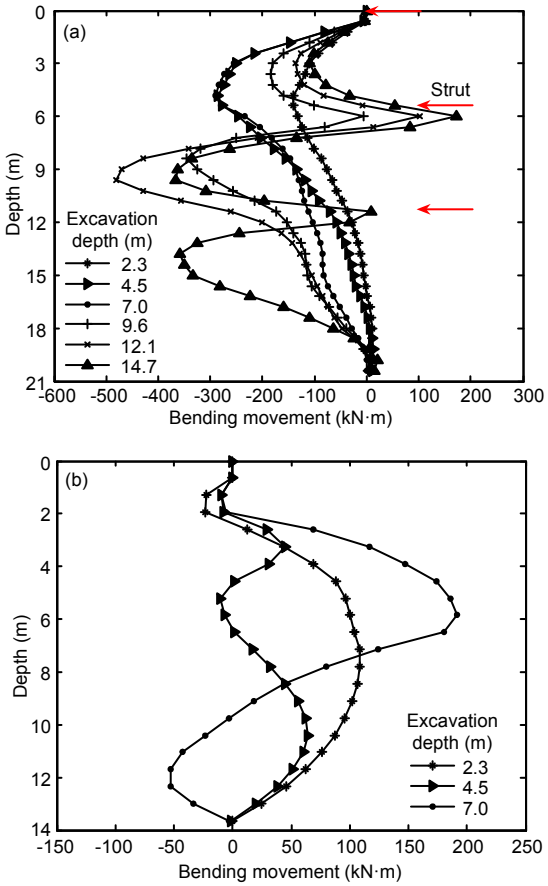

Fig. 10 Bending moments in pile A (a) and pile B (b) at different excavation depths

5.2 Internal forces analysis

As the earth pressure difference between both sides of the pile walls increases, the maximum bending moments of vertical piles A and B, corresponding to rotation about *y*-, *x*-axis of the pile, respectively, increase with the progress of excavation (Fig. 10). At the lower tip of both piles, bending moments become null and are similar with those of the pile top. In addition, on the bending moment curves of pile A, there are some clear inflection points that occur near the location of the struts. The strut can play a regulatory role in the distribution of bending moments and be an effective restraint for bending deformation of the piles. Thus, it is necessary to account for a proper arrangement of the strut locations to reduce the bending moments.

The axial loads in the struts for each stage are shown in Fig. 11. When the excavation reaches the location of a given strut, its axial load becomes relatively large, while the variation in other previously installed struts is moderated. The axial load in the top strut increases at the second stage, and then decreases at the later stages. At the end of the excavation, the maximum axial load appears in the bottom strut, which corresponds to the pile deformation law that the maximum deflection occurs near the excavation surface, as shown in Fig. 9a.

The histogram (Fig. 12) shows the axial loads in three struts at the cross section, together with the average loads of the left-sided ones. As illustrated from comparison, the axial loads are unequal to each other and the values near the convex corner are generally larger than those of the left struts, on average. As there are two free excavated sides at the convex location, a large tensile stress resulting from unloading could easily lead to a wedge-shaped

failure. Consequently, the development of the pile deformation results in larger axial loads in the strut, which makes the junction a key location in strut design.

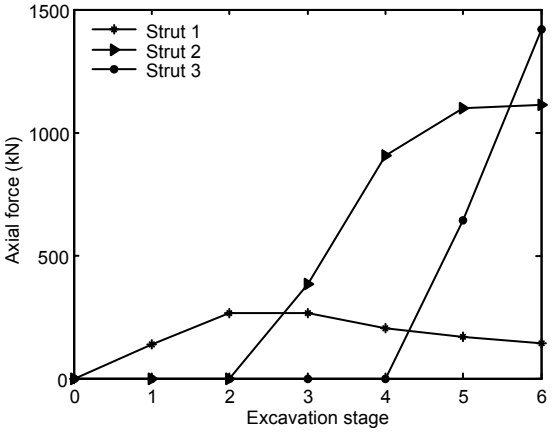

Fig. 11 Axial loads in struts

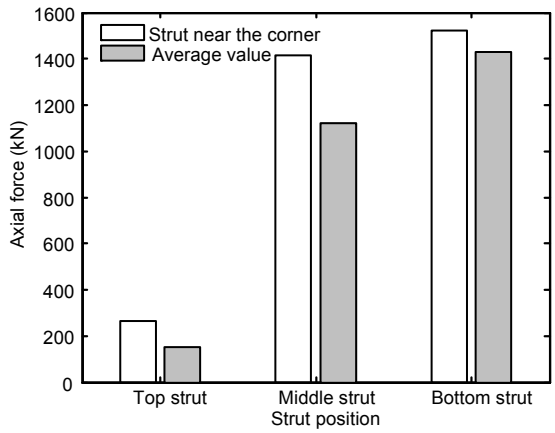

Fig. 12 Comparison of axial loads in strut

5.3 Influence of the parameter κ on excavation behavior

Since the excavation involves unloading in both horizontal and vertical directions during the soil removal, the horizontal stresses decrease in the soil elements and the subsequent soil resilience in both active and passive zones drives lateral displacements of the retaining structures. Fig. 13 illustrates the effect of the slope κ of an elastic swelling line on the movement patterns of pile A at the final stage for a given slope λ of a normal consolidation line. As shown in this figure, an increase of κ from $\lambda/6$ to $\lambda/3$ results in substantial increases in the pile deformations by approximately twice the lateral movements. The soil parameter κ significantly affects the pattern of the pile wall deformation profiles, and ideally, should be estimated based on an isotropically loaded triaxial test with several unloading excursions.

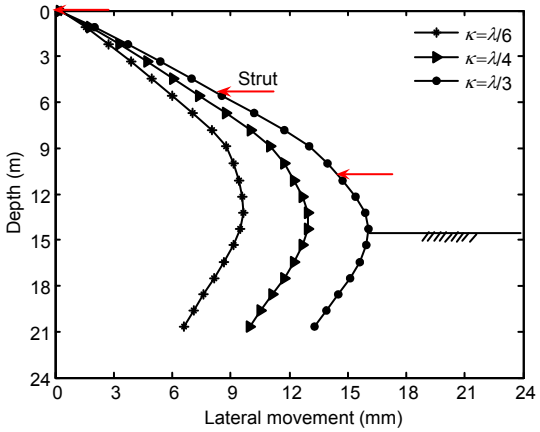

Fig. 13 Comparison of pile deformations under different κ (pile A)

Fig. 14 displays the contours of ground surface settlements at the end of excavation (i.e., stage 7) for the 3D analyses with κ/λ=1/4 and 1/6. A settlement trough can generally be observed in the vicinity of the pit and the maximum values in the cross section are explicitly higher than those in the central sections of the excavation. In addition, they follow a relationship similar to that of the pile wall deflections, as well as that of different slopes κ of elastic swelling lines. Examining the influence zone of the surface settlements, there is still a 3 mm settlement extending up to about five times the excavation depth ($5H$). Nevertheless, as indicated in Hsieh and Ou (1998) for both spandrel and concave settlement profiles through several case histories, the surface settlements nearly decrease to zero at the distance of approximately four excavation depths ($4H$) behind the pile wall. The cause of the divergence is that the existence of the convex corner expands the influence of the settlement trough. Moreover, on the other hand, the MCC model used in the numerical simulation does not take into account the nonlinear behavior of the soil stiffness under the small strain, which makes the far-field displacement non-convergent at the end of the settlement trough.

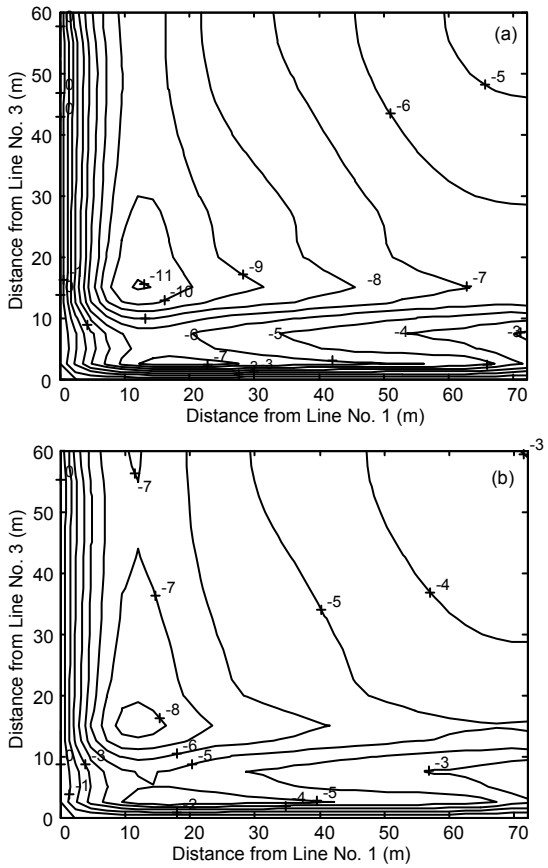

Fig. 14 Surface settlement contours at the end of excavation with $\kappa=\lambda/4$ (a) and $\kappa=\lambda/6$ (b) (unit: mm)

5.4 Influence of constitutional models

It is desirable to compare the numerical outputs to evaluate the ability of the various soil models to describe the overall soil behavior. Fig. 15 shows a comparison between the results of the MCC and MC model simulations. As shown in Figs. 15a and 15b, the pile deflections and surface displacement predicted by the MCC model are generally close to the actual situation, which reveals the capability of describing the excavation behavior with unloading. Meanwhile, a large upward movement of ground surface together with a maximum pile deflection occurring at the pile tip is predicted by the MC model, an illogical pattern that deviates significantly from reality. The reason is that the loading-unloading criterion to reach different values of the soil stiffness in the active and passive zones is not introduced in the MC model and the impact of stress path is also not considered. These limitations can produce a large rebound deformation at the bottom of the excavation and subsequently induce an unrealistically large lateral movement, especially at the tip. Additionally, due to the hypothesis of perfect adhesion at the soil-pile contact, vertical pile wall movements, from the bottom heaves caused by the removal of the excavated masses are induced which in turn are reflected in ground surface heaves. As mentioned by Jardine *et al*. (1986), the vertical movement of the retained soil surface obtained by a simple elastic-plastic soil model is not generally very realistic.

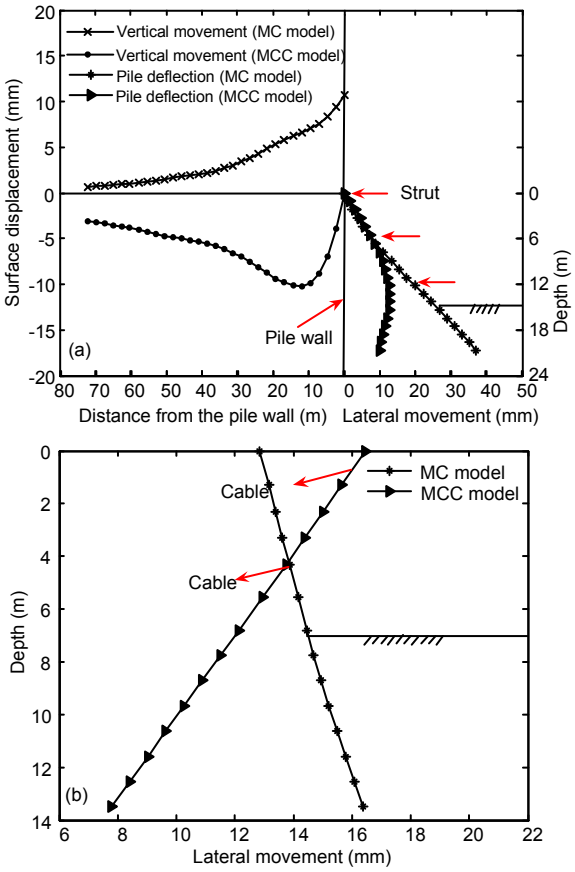

Fig. 15 Deformations of pile A (a) and pile B (b) predicted by the MC model and MCC model, respectively

On the contrary, the MCC model in which stress varies as an exponential function of volumetric strain, takes into account the effects of the consolidation pressure and allows plastic volume changes. Furthermore, the soil stiffness of unloading, by adjusting the parameters κ and λ, is larger than that of loading, which is conform to the approximate reality. Thus, the MCC model would be highly advantageous to investigate the pile wall deflection and ground settlement associated with excavation.

In footings and excavations, the non-linear small strain stiffness properties, namely the soil shear stiffness, actually reduce rapidly as the strain increases, and appear to have a significant influence on interpretation in soil-structure interactions (Jardine *et al*., 1986). However, the MCC model overestimates the soil shear strength, which would lead to an over-stiff response for the soil on the passive side during the shear process (Yin, 2010). Accounting for the deficiency of the common models on this aspect, the HSS model introduced by Benz (2007) and a special type of models based on the theory of "hypoplasticity" (Masin, 2005) were developed sequentially. These advanced models are capable of simulating the soil characteristics, such as the soil hardening by shearing and compression, loading-unloading criterion, and the non-linear small strain stiffness. They are more accurate in predicting lateral and vertical movements. Unfortunately, the models have not been included in the analysis software FLAC^{3D} adopted in this study, and further research needs to address this.

6 Conclusions

The objective of this paper is to investigate the convex effect in the crossing excavation with the case of the Qingdao North Metro Station, China, and provide guidance for the most appropriate approach to be used in 3D numerical analyses. In this study, the corner effect, with a series of numerical cases of various angles on the excavation behavior, is preliminarily explained. Then the effects of two alternative constitutive assumptions, together with the parameter study of the soil resilience characteristic on the overall response of the propping system, are discussed. The following main conclusions can be drawn from the study.

1. The displacements at the intersection during crossing excavation decrease with an increase in the crossing angles, and the obtuse angle is recommended for primary crossing design (if available).

2. The pile wall deflections at various distances from the cross section in metro Line No. 1 seem to be equal, while the axial loads of the struts are unequal to each other and those near the intersection are generally larger than that, on average, of the left struts. Furthermore, the embedded depth of the pile wall with the propping type of struts has little impact on the lateral deflection.

3. The slope κ of elastic swelling line has a significant influence on the magnitude and distribution of pile and ground movement characteristics, and slight deformation resilience after unloading can obviously reduce the ground settlement, and enhance the excavation stability.

4. The MCC model used in this study, which is capable of describing the loading-unloading criterion and evaluating the stiffness under various stress states, can yield a relatively reasonable degree of accuracy to make an estimate of pile deflection and ground surface movement profiles. Nevertheless, the most commonly used MC model, which employs a single stiffness without considering the diversity under various stress states, cannot produce satisfactory results in estimating ground movement, and is not recommended for excavation analysis.

References

Benz, T., 2007. Small-Strain Stiffness of Soils and Its Numerical Consequences. PhD Thesis, Stuttgart University, Germany.

Finno, R.J., Roboski, J.F., 2005. Three-dimensional responses of a tiedback excavation through clay. *Journal of Geotechnical and Geoenvironmental Engineering*, **131**(3): 273-283. [doi:10.1061/(ASCE)1090-0241(2005)131:3(273)]

Gourvenec, S.M., Powrie, W., 2000. Three-dimensional finite-element analysis of embedded retaining walls supported by discontinuous earth berms. *Canadian Geotechnical Journal*, **37**(5):1062-1077. [doi:10.1139/t00-033]

Hou, Y.M., Wang, J.H., Zhang, L.L., 2009. Finite-element modeling of a complex deep excavation in Shanghai. *Geotechnical and Geological Engineering*, **4**:7-16. [doi:10.1007/s11440-008-0062-3]

Hsieh, P.G., Ou, C.Y., 1998. Shape of ground surface settlement profiles caused by excavation. *Canadian Geotechnical Journal*, **35**(6):1004-1017. [doi:10.1139/t98-056]

Itasca Consulting Group, Inc., 2005. Fast Lagrangian Analysis of Continua, Version 5.0 User Manual. Minneapolis, USA.

Jardine, R.J., Potts, D.M., Fourie, A.B., Burland, J.B., 1986. Studies of the influence of non-linear stress-strain characteristics in soil-structure interaction. *Geotechnique*, **36**(3):377-396. [doi:10.1680/geot.1986.36.3.377]

Kung, G.T., Jheng, U.Z., 2010. Evaluation of analyzing excavation-induced wall deflection and ground movement using hardening soil models. *Chinese Journal of Geotechnical Engineering*, **32**(Supp. 2):175-178 (in Chinese).

Masin, D., 2005. A hypoplastic constitutive model for clays. *International Journal for Numerical and Analytical Methods in Geomechanics*, **29**(4):311-336. [doi:10.1002/nag.416]

Nakai, T., Farias, M.M., Bastos, D., Sato, Y., 2007. Satosimulation of conventional and inverted braced excavation using subloading t_{ij} model. *Soils and Foundations*, **47**(3):597-612. [doi:10.3208/sandf.47.597]

Ng, C.W.W., Yan, R.W.M., 1999. Three-dimensional modeling of a diaphragm wall construction sequence. *Geotechnique*, **49**(6):825-834. [doi:10.1680/geot.1999.49.6.825]

Ou, C.Y., Shiau, B.Y., 1998. Analysis of the corner effect on excavation behaviors. *Canadian Geotechnical Journal*, **35**(3):532-540. [doi:10.1139/t98-013]

Ou, C.Y., Chiou, D.C., Wu, T.S., 1996. Three-dimensional finite element analysis of deep excavation. *Journal of Geotechnical and Geoenvironmental Engineering*, **122**(5):473-483. [doi:10.1061/(ASCE)0733-9410(1996)122:5(337)]

Ou, C.Y., Teng, F.C., Wang, I.W., 2008. Analysis and design of partial ground improvement in deep excavations. *Computers and Geotechnics*, **35**(4):576-584. [doi:10.1016/j.compgeo.2007.09.005]

Roscoe, K.H., Burland, J.B., 1968. On the Generalised Stress-Strain Behaviour of Wet Clay. Engineering Plasticity. Cambridge, Cambridge University Press, New York, p.535-609.

Tang, Y.G., 2011. Probability-based method using RFEM for predicting wall deflection caused by excavation. *Journal of Zhejiang University-SCIENCE A (Applied Physics & Engineering)*, **12**(10):737-746. [doi:10.1631/jzus.A1100028]

Tang, Y.G., Kung, G.T.C., 2010. Investigating the effect of soil models on deformations caused by braced excavations through an inverse-analysis technique. *Computers and Geotechnics*, **37**(6):769-780. [doi:10.1016/j.compgeo.2010.06.003]

Viggiani, G., Tamagnini, C., 2000. Ground movements around excavations in granular soils: a few remarks on the influence of the constitutive assumptions on FE predictions. *Mechanics of Cohesive-Frictional Materials*, **5**(5):399-423. [doi:10.1002/1099-1484(200007)5:5<399::AID-CFM101>3.0.CO;2-R]

Wu, Z.M., Tu, Y.M., 2007. Space effect of soil-nailing excavation protection. *Rock and Soil Mechanics*, **28**(10):2178-2182 (in Chinese).

Xu, Z.H., Wang, W.D., 2010. Selection of soil constitutive models for numerical analysis of deep excavations in close proximity to sensitive properties. *Rock and Soil Mechanics*, **31**(1):258-326 (in Chinese).

Yin, J., 2010. Application of hardening soil model with small strain stiffness in deep foundation pits in Shanghai. *Chinese Journal of Geotechnical Engineering*, **32**(Supp. 1):166-172 (in Chinese).

Zdravkovic, L., Potts, D.M., John, H.D.S.T., 2005. Modelling of a 3D excavation in finite element analysis. *Geotechnique*, **55**(7):497-513. [doi:10.1680/geot.2005.55.7.497]

Zhang, M., Song, E., Chen, Z., 1999. Ground movement analysis of soil nailing construction by three-dimensional (3-D) finite element modeling (FEM). *Computers and Geotechnics*, **25**(4):191-204. [doi:10.1016/S0266-352X(99)00025-7]